geoconvention
Virtual Event
September 13 - 15
2021

Reconstructing Hydraulic-Fracture Induced Strain from Microseismicity

Adam M. Baig, Ben Witten, Aaron Booterbaugh
Nanometrics

Introduction

Latest results comparing microseismic event distributions due to hydraulic fracture with mined-back core directly sampling these fractures indicates that the microseismic response is not a direct tie to the fluid and proppant intrusion into the reservoir (Gale et al., 2018, Stegent and Candler, 2018). We consider that microseismicity itself can be used as a proxy for the strain state about the reservoir, which is an output of geomechanical fracture models. So, instead of viewing (perhaps incorrectly) hypocenters as waypoints along the hydraulic fracture, the fracture growth could be constrained by matching strain fields between microseismic prediction and geomechanical models. Using seismicity to calculate strain has been used to relate to crustal geodynamics and mining scenarios for decades (e. g. Bailey et al., 2009, Middleton et al., 2018, Ward, 1998, Urbancic et al., 1997), and is readily applicable to other fields.

The moment tensor is proportional to the strain rate tensor through the rock properties of the medium. Using a mixed array of near-surface, borehole-deployed geophones and surface geophone arrays, a multi-well completion was monitored for microseismicity. Moment tensors are inverted from a novel workflow that compares the goodness of fit of the amplitude data with noise data to understand the statistical significance of the solutions. Because first motions are infrequently observed, assumptions are made on the state of stress, to select individual moment tensors from their mirror-images, which otherwise equally satisfy the data. For the entire completion, over 17000 events are detected and located from the mixed array. All events are inverted for moment tensors, obtaining a set of over 2700 with greater than 95% confidence. Over the reservoir, events are grouped by proximity and the aggregate tensorial strain field is obtained from the microseismicity and assigned to various grid points.

The strain response through DAS in the immediate vicinity of a fiber-optic cable has been well-understood in the last few years and many interesting examples have been published (e.g. Jin and Roy, 2017). Our use of microseismicity to describe the strain tensor is complementary to this approach. The lack of well-resolved mechanisms for many events, to say nothing of the events below the detectability threshold, causes us to recognize the microseismic strain in this workflow should underestimate the total strain. Using DAS to calibrate this underestimation by extracting the axial strain along the well opens the door to being able to accurately estimate the magnitude of the strains over the entire reservoir. The gridded nature of the resulting fields makes them immediately comparable to modelling results suggesting that this distillation of the microseismic response can be directly incorporated into geomechanical calibration workflows.

Strain and Seismicity

A quantitative framework for describing variations in stress and strain can be formulated by considering the effect that a group of microseismic events have on a volume of rock. The

developments in this section largely follow from Kostrov (1974) and Kostrov and Das (1988) but we feel that it is useful to restate these derivations. Due to the fundamental nature of Kostrov's 1974 work in introducing these techniques to the West this methodology has become known in the literature as “Kostrov summation” (although he cited Riznichenko's 1965 Russian-language paper). Due to the importance of the distinction between moment tensors and potency tensors in anisotropic media (e.g. Chapman and Leaney, 2012, Grechka, 2020), and the ubiquity of anisotropic rocks in reservoirs we reframe these strain relationships in terms of potency.

Kostrov and Das (1988) present a straightforward derivation for how moment tensor data within a volume relate to the strain of that volume. Largely in the footsteps of their work, we consider a grouping of events in a volume, ΔV, that occur over a time nucleating on planes of weakness described by unit normal vectors, $\hat{\mathbf{n}}^{(i)}$, and slip vectors $\mathbf{s}^{(i)}$. The average strain within a volume is described in their eq. 4.5.13, referring to figure 1 for the definitions of various quantities, as:

$$\boldsymbol{\epsilon} = \frac{1}{\Delta V}\sum_{\kappa}\int_{\nu^{(\kappa)}} \frac{\mathbf{s}^{(\kappa)}\hat{\mathbf{n}}^{(\kappa)} + \hat{\mathbf{n}}^{(\kappa)}\mathbf{s}^{(\kappa)}}{2} d\nu^{(\kappa)}. \tag{1}$$

In full generality, both the slip vectors and normal vectors can be functions of position on the surface, which need not be a penny-shaped crack, although only in rare cases can these variations be resolved. The deformation in the volume due to these events is described by a strain tensor, $\boldsymbol{\epsilon}$ and graphically depicted by the non-orthogonality of the parallelepiped axes. Recognizing the terms under the summation as potency tensors, $\mathbf{P}$, for each event (Ampuero and Dahlen, 2005), the strain of a volume can be evaluated as:

$$\boldsymbol{\epsilon} = \frac{\sum_{\kappa}\mathbf{P}^{(\kappa)}}{2\Delta V} \tag{2}$$

and the strain-rate is similarly arrived at as:

$$\dot{\boldsymbol{\epsilon}} = \frac{\sum_{\kappa}\mathbf{P}^{(\kappa)}}{2\Delta V \Delta t}. \tag{3}$$

Because we choose to use the potency tensor instead of the moment tensor, $\mathbf{M}$, (as Kostrov, 1974 does) at the outset, we avoid needing to untangle the moment tensor from the stiffness tensor, $\mathbf{C}$, naturally handling arbitrary anisotropy, and generalizing the derivation for non-double-couple sources, where the slip vector, $\mathbf{s}$, (averaged over each individual crack) is not necessarily perpendicular to the fault/crack plane normal, $\hat{\mathbf{n}}$. Indeed, this parametrization in terms of potency has been suggested already in the mining industry (e.g. Mendecki et al., 2010).

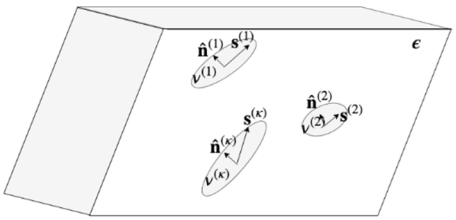

Figure 1. A volume, ΔV of rock contains a number of microseismic events occurring over a time Δt. Each event is described by a surface, ν^i, with slip vector $\mathbf{s}^i$, and unit normal vector, $\hat{\mathbf{n}}^i$.

We recognize the strain reconstructed in this fashion from microseismicity should always underestimate the total strain due to the events that are below the detectability threshold, and the failure to account for undetectable events or true aseismic strain (creep). Ward (1998) discusses on continental scales the comparison between Kostrov summation strain values and the values

obtained from geological and geodetic values and finds underestimation of deformation due to this lack of a complete enough catalog. The formulations in equations 2 and 3 on the surface seem straightforward, but the estimation of the volume ΔV is non-trivial. For example, one could make numerous choices on how to define this volume given a group of event hypocenters as the smallest sphere that circumscribes them, their convex hull, the best-fitting ellipsoid, or numerous other choices. Each choice seems reasonable (at least to these authors), but will result in different magnitudes of the resultant strain. We suggest that these ambiguities can be captured by a scalar factor, that the "true" strain, $\boldsymbol{\epsilon}_{\text{true}}$ in the reservoir is related to the seismic strain as:

$$\boldsymbol{\epsilon}_{\text{true}} = \zeta \boldsymbol{\epsilon}. \tag{4}$$

by the scalar, ζ factor and leave open the question of what is the appropriate volume that should be used and to what degree undetectable events and aseismic creep contribute to the strain calculation. Explicitly, we assume ζ is constant across the seismogenic volume for a dataset with a completeness magnitude imposed, which is admittedly questionable, especially in the face of variable lithology.

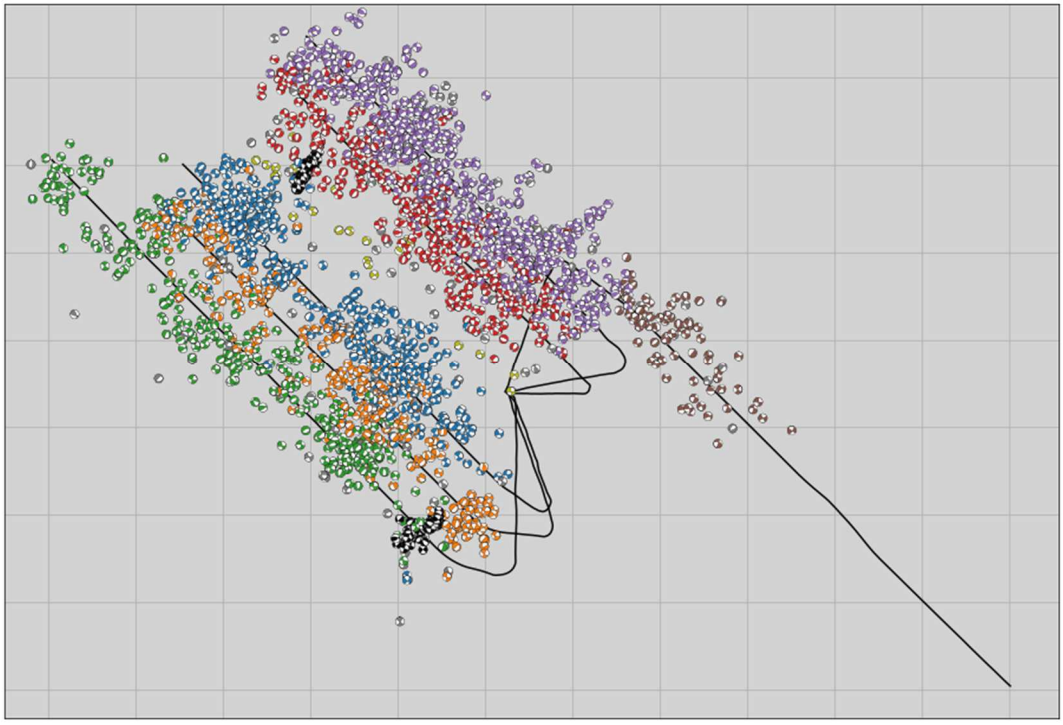

Figure 2 The completion of 6 wells was monitored for microseismicity and 2752 moment tensors were inverted with a confidence of greater than 95%. The grid spacing is 250m × 250m. Events are colored by treatment well, except for the black colors reserved for identified structures responding away from the injection.

Hydraulic Completion Example

We examine the hydraulic pad completion of six wells in a North-American shale play monitored from a heterogeneous network of shallow-borehole geophones and surface-deployed "superstation" patches. Witten et al. (2021) compare the signals on both of these types of station geometries. Over the course of the completion, over 17000 events were recorded and confidently

located. Moment magnitudes were assigned following the procedure outlined by Baig et al. 2019, and ranged from $-1.7 < M_W < 0.8$ with a magnitude of completeness of $M_C = -1.3$.

We use the signed amplitudes of the first motions of recorded *P* waves to invert for moment tensors of each event and then assign it a confidence based on the similarity of the fit with a distribution of inversions from noise (Witten et al., 2020). Because the first motions are generally not as clear as the peak amplitudes, and may in fact be opposite in sign, we admit that the mechanisms may have a sign ambiguity that we resolve by appealing to the notions of what the dominant stress state is (Baig et al., 2020).

The conversion to potency tensors is performed by the contraction of the compliance tensor with the resolved moment tensors.

$$\mathbf{P} = \mathbf{S} : \mathbf{M} \tag{5}$$

There is no reason to solve the moment tensor and then apply the compliance to obtain the potency tensor rather than simply solve for the potency tensors *ab initio*, this ordering reflects our particular order of operations. The coefficients of the compliance tensor, $\mathbf{S}$ are determined from an optimization of the *P*-wave traveltimes assuming a layered VTI model and using a correlation of the stiffness parameters (Yan et al., 2019) to obtain a value on the otherwise unconstrained parameters on the tensor (C_{66}, S_{66} in Voigt notation). The potency tensors constructed can be used with application of equation 5 to map the co-seismic strain tensor in the reservoir from the events.

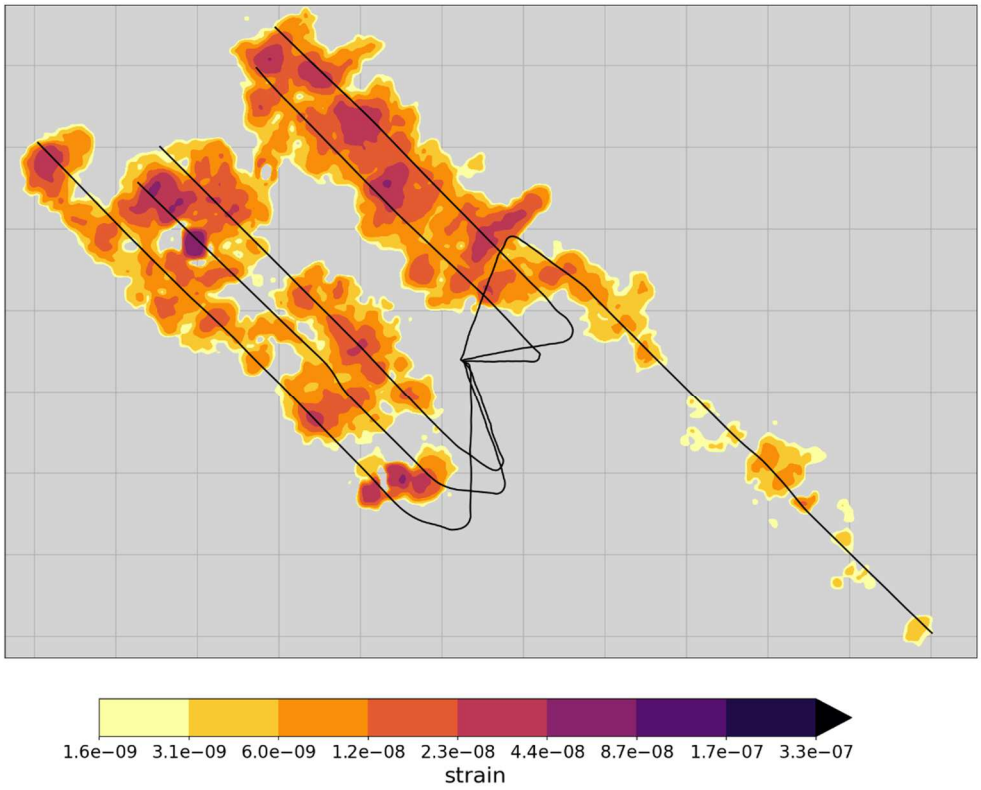

Figure 3. The magnitude of strain is contoured over the reservoir for the six wells. The grid spacing is 250m × 250m.

Strain Response and Constructing a Synthesized DAS response

If we concern ourselves only with the magnitude of the strain and not the orientations of the strain tensor, then we obtain a measure of total motion that has been experienced by the reservoir. The norm of the strain tensor, relates to the scalar potency, approximately equivalent to the seismic moment over shear modulus. As such, we are not restricted to using the events with confident moment tensors. In figure 3 this quantity is contoured in the reservoir and show clear differences across the pad. The Northeast wells show that there is a consistent degree of deformation occurring over the reservoir. in contrast, the wells to the Southwest show a large degree of inconsistency and presumably not an even degree of stimulation. The one well stimulated on the south of the pad is not as effectively stimulated in this case either.

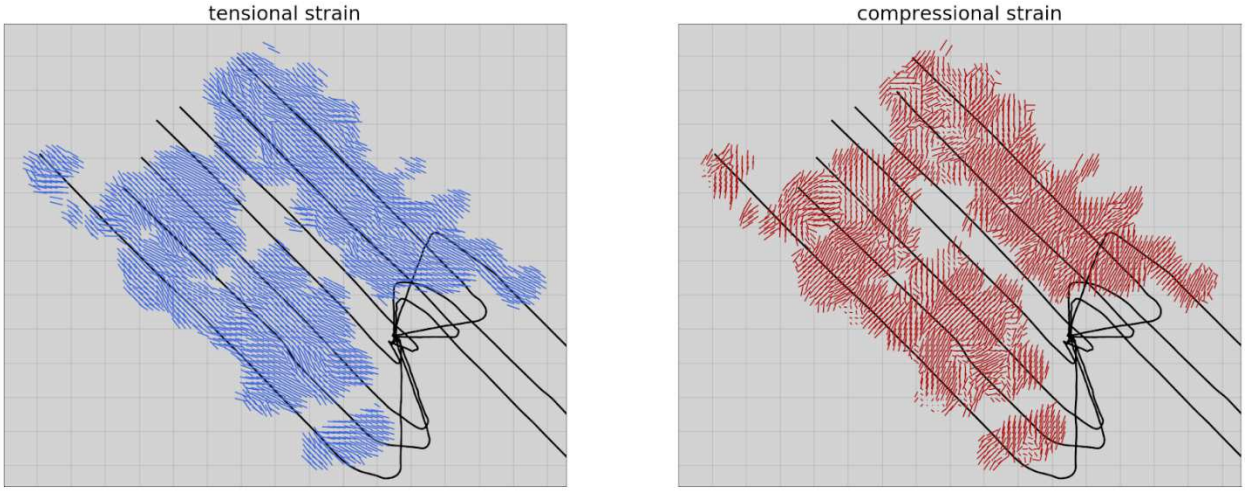

Figure 4. The orientations of the tensional (left) and compressional (right) strain axes are plotted. The length of the vector corresponds to the relative horizontal component, as if the vector is being looked down. The grid spacing is 250 m × 250 m.

Figure 4 shows the orientations of the strain tensor are determined from the eigenvectors of the gridded strain tensors over the reservoir. Because moment tensors are only well resolved over the north side of the pad, we only examine orientation variations between the Northeast and Southwest wells. The tensional strain axes are very closely aligned with the wells for the Northwest wells relative to the Southwest wells indicating that the strain on the Northwest is very consistent with opening events. Compressional strain is less organized, but again the Southwest wells show more heterogeneity. This general disorganized strain field in the Southwest might be responding to geological heterogeneity in this area.

Distributed acoustic sensing also yields estimates of the strain field: that is the change in length along the cable between sample points. In terms of the total strain tensor, DAS resolves one of the diagonal components of the tensor, aligned along the cable itself. We can specify this component to be ϵ_{11} working in a coordinate system where the first direction is aligned along the arclength of the hypothetical cable (which we will assume to be equivalent to the measured depth

of the well). According, we can compute this "along-well" volumetric strain component using the microseismic response.

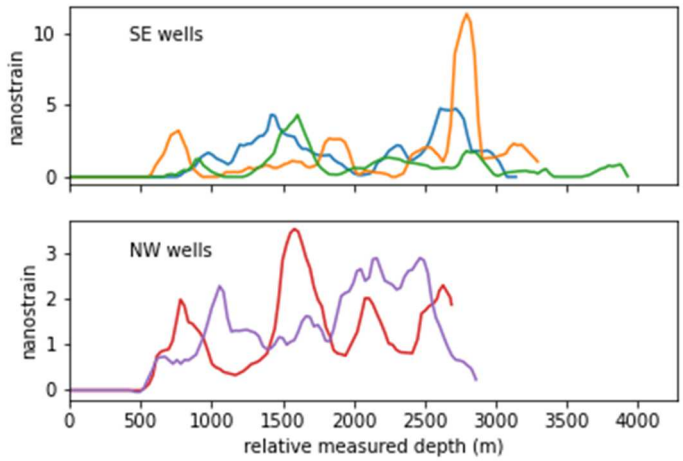

Figure 5. Along-well strain as computed from the potency tensors for both sets of wells on the North half of the pad.

In figure 5 we plot the along-well strain for the different wells on the North half of the pad. The general inconsistent response of the Southwest wells relative to the Northeast wells indicates potentially the more intermittently stimulated nature of the former set of wells. The component of the strain tensor we plot here is the same one that would result from a distributed acoustic sensing system deployed along the wells. These responses could be as functions of time well (isolating events that occur in given time windows) as many DAS results are presented on a stage-by-stage scale (e.g. Jin and Roy, 2017).

Discussion

We have shown how to use microseismic data to construct a tensorial strain field across a volume, acknowledging that because we are only able to reconstruct strain tensors for the events that we can invert moment tensors from, the response we reconstruct is a scaled version of the actual strain. By translating this response into the component that would be measured through low-frequency DAS, we offer a workflow that can potentially be followed to calibrate this scaling factor. In doing so, integrating the DAS and microseismic responses together would enable a calibrated strain tensor to be determined over the reservoir (or the seismogenic region of interest).

We would not necessarily expect microseismic and DAS strain responses to be exactly correlated. Notably we anticipate the need to adjust the responses to the same spatial wavenumber. The location error of microseismic events needs to be accounted for in this workflow, and reconciled with the DAS gauge length through a tuning of smoothing parameters. We note that Kostrov summation is essentially an averaging procedure and we might expect a more accurate image of strain then the nominal microseismic location error might suggest, however these errors may result in a larger averaging volume systematically underestimating the strain. Geological factors

might also be responsible for decorrelation microseismic and DAS strain. The ability for some formations to deform plastically versus brittly (Eyre et al., 2019) is one salient reason that could tie back to the mineralization of different formations and potentially even within formations.

Conclusions

We show how microseismicity can be used to construct a strain response comparable to the responses obtained through DAS. Such applications of using moment tensors to compare with absolute measurements of deformation mirror developments in crustal seismology and the mining industry. In doing so, we suggest how these two technologies can complement each other to reconstruct the full strain tensor field over a reservoir that provides a suitable point of comparison for geomechanical modelling of fracturing on a gridded computational domain.

Acknowledgements

We are grateful to the owners of the data for allowing us their use and to our diligent colleagues at Nanometrics without whose work to process these data none of this work would have been possible.

References

Ampuero, J.-P., and Dahlen, F. A., 2005, Ambiguity of the Moment Tensor, *Bull. Seism. Soc. Am.*, **95**, pp. 390-400.

Baig, A. M., Witten, B., Karimi, S., Baturan, D., and Yenier, E., 2019, Magnitude Calibration of Imaging-Based Microseismic Locations, Presented at the 89th Annual Society of Exploration Geophysics International Meeting, San Antonio.

Baig, A. M., Witten, B., and Karimi, S., 2020, Quality Control of Microseismic Moment Tensors from Surface-Based Acquisitions, presented at Geoconvention, Calgary.

Bailey et al., 2009, Patterns of co-seismic strain computed from southern California focal mechanisms, *Geophys. J. Int.*, **177**, pp 1015-1036, doi: 10.1111/j.1365-246X.2009.04090.x

Chapman, C. H. and Leaney, W. S., 2012, A new moment-tensor decomposition for seismic events in anisotropic media, *Geophys. J. Int.*, **188**, pp 343-370, doi: 10.1111/j.1365-246X.2011.05265.x

Eyre, T. S., Eaton, D. W., Garagash, D. I., Zecevic, M., Venieri, M., Weir, R., and Lawron, D. C., 2019, The role of aseismic slip in hydraulic fracturing-induced seismicity, *Science Advances*, **5**, eaav7172, doi:10.1126/sciadv.aav7172

Gale, J. F. W. & Elliott, S. & Laubach, S. E. 2018. Hydraulic Fractures in Core From Stimulated Reservoirs: Core Fracture Description of HFTS Slant Core, Midland Basin, West Texas presented at Unconventional Resources Technology Conference, Houston doi: 10.15530/urtec-2018-2902624.

Grechka, V. 2020, Moment tensors of double-couple microseismic sources in anisotropic formations, *Geophysics*, **85**, pp 1-43, doi: 10.1190/geo2019-0471.1

Jin, G. and Roy, B., 2017, Hydraulic-fracture geometry characteristization using low-frequency DAS signal, *The Leading Edge*, **36**, pp. 975-980, doi:https://doi.org/10.1190/tle36120975.1

Kostrov, B.V., 1974. Seismic moment and energy of earthquakes and seismic flow of rock, *Phys. Solid Earth*, **1**, 23–40.

Kostrov and Das, 1988, *Principles of Earthquake Source Mechanics,* Cambridge University Press, Cambridge

Mendecki, A. J., Lynch, R. A., Malovichko, D. A., 2010, Routine micro-seismic monitoring in mines, Presented at Australian Earthquake Engineering Society, Perth, Western Australia.

Middleton, T. A., Parsons, B., Walker, R. T., 2018, Comparison of seismic and geodetic strain rates at the margins of the Ordos Plateau, northern China, *Geophys. J. Int.*, **212**, pp 988-1009, doi:10.1093/gji/ggx446

Riznichenko, Yu. V.,1965, Seismic rock Flow, in: Dynamics of the Earth's Crust, Nauka, Moscow (in Russian)

Stegent, N. and Candler, C., 2018, Downhole microseismic mapping of more than 400 fracturing stages on a multiwell pad at the Hydraulic Fracturing Test Site (HFTS): discussion of operational challenges and analytic results, presented at Unconventional Resources Technology Conference, Houston doi: 10.15530/urtec-2018-2902311

Urbancic, T. I, Trifu, C.-I., and Shumila, V., 1997, Investigating the extent of excavation influence using deformation state analysis, in: Rockbursts and Seismicity in Mines, edited by Gibowicz and Lasocki, Balkema, Rotterdam

Ward, S. N., 1998, On the consistency of earthquake moment rates, geological fault data, and space geodetic strain: the United States, *Geophys, J. Int.*, **134**, pp. 172-186

Witten, B., Baig, A. M., Karimi, S., and Purdue, G., 2020, Surface microseismic acquisition and processing with a lightweight array, presented at 90th Annual Society of Exploration Geophysics International Meeting, Houston

Witten, B., Baig, A. M., and Vaezi, Y., 2021, A comparison of collocated surface and shallow borehole arrays for microseismic monitoring, presented at 91st Annual Society of Exploration Geophysics International Meeting, Denver

Yan, F., Vernik, L., Han, D.-H.., 2019, Relationship between the anisotropy parameters for transversely isotropic mudrocks, *Geophysics*, **84**, pp. MR195-MR203, doi: 10.1190/GEO2019-0088.1